Giant Overlap between the Magnetic and Superconducting Phases of $CeAu_2Si_2$ under Pressure

Z. Ren,[1] L. V. Pourovskii,[2,3] G. Giriat,[1] G. Lapertot,[4,5] A. Georges,[2,6,1] and D. Jaccard[1*]

[1]*DPMC-University of Geneva, 24 Quai Ernest-Ansermet, 1211 Geneva 4, Switzerland*
[2]*Centre de Physique Théorique, CNRS, École Polytechnique, 91128 Palaiseau, France*
[3]*Department of Physics, Swedish e-science Research Centre (SeRC), Chemistry and Biology (IFM), Linköping University, SE-58183 Linköping, Sweden*
[4]*University of Grenoble Alpes, INAC-SPSMS, F-38000 Grenoble, France*
[5]*CEA, INAC-SPSMS, F-38000 Grenoble, France*
[6]*Collège de France, 11 place Marcelin Berthelot, 75005 Paris, France*

(Received 5 June 2014; published 26 September 2014)

High pressure provides a powerful means for exploring unconventional superconductivity which appears mostly on the border of magnetism. Here, we report the discovery of pressure-induced heavy-fermion superconductivity up to 2.5 K in the antiferromanget $CeAu_2Si_2$ ($T_N \approx 10$ K). Remarkably, the magnetic and superconducting phases are found to overlap across an unprecedentedly wide pressure interval from 11.8 to 22.3 GPa. Moreover, both the bulk T_c and T_M are strongly enhanced when increasing the pressure from 16.7 to 20.2 GPa. T_c reaches a maximum at a pressure slightly below $p_c \approx 22.5$ GPa, at which magnetic order disappears. Furthermore, the scaling behavior of the resistivity provides evidence for a continuous delocalization of the Ce $4f$ electrons associated with a critical end point lying just above p_c. We show that the maximum T_c of $CeAu_2Si_2$ actually occurs at almost the same unit-cell volume as that of $CeCu_2Si_2$ and $CeCu_2Ge_2$, and when the Kondo and crystal-field splitting energies become comparable. Dynamical mean-filed theory calculations suggest that the peculiar behavior in pressurized $CeAu_2Si_2$ might be related to its Ce-$4f$ orbital occupancy. Our results not only provide a unique example of the interplay between superconductivity and magnetism, but also underline the role of orbital physics in understanding Ce-based heavy-fermion systems.

DOI: 10.1103/PhysRevX.4.031055

Subject Areas: Condensed Matter Physics, Strongly Correlated Materials, Superconductivity

I. INTRODUCTION

Superconductivity (SC) and magnetism were long thought to be antagonistic. In this context, the discovery 22 years ago that high pressure turns a magnetically ordered heavy-fermion (HF) compound, namely, $CeCu_2Ge_2$, into a superconductor has attracted much attention in the condensed matter physics community [1]. Since then, high-pressure studies of Ce-based HFs have revealed a number of superconductors such as $CePd_2Si_2$ [2], $CeIn_3$ [3], $CeRhIn_5$ [4], and, more recently, $CePt_2In_7$ [5]. In all known cases, SC emerges in the vicinity of a magnetic-nonmagnetic phase boundary, and most often competes for stability with magnetic order, except in a few examples where both states coexist within a narrow pressure range [6].

$CeCu_2Ge_2$ is an isostructural sister compound of the first discovered HF superconductor $CeCu_2Si_2$ [7], which exhibits a second superconducting phase under pressure with a higher T_c [8–12]. Remarkably, $CeCu_2Ge_2$ shares the same phase diagram as $CeCu_2Si_2$ when pressurized above ~10 GPa, where magnetism disappears [9,13]. Indeed, both compounds feature the existence of connected low- and high-pressure superconducting phases associated with two critical points of different origins. Moreover, the partial substitution of Si by Ge in $CeCu_2Si_2$ results in the splitting of the initially joined superconducting phases into two distinct domes due to disorder-induced pair breaking [14].

Despite three decades of efforts, the underlying mechanisms for the two superconducting phases are still poorly understood. On one hand, it is widely believed that SC at low pressure is mediated in these systems by critical spin fluctuations [15,16]. However, this view was very recently challenged by a thermodynamical study that points to multiband SC with a full energy gap in $CeCu_2Si_2$ at ambient pressure [17]. On the other hand, there is no general consensus that critical valence fluctuations are responsible for high-pressure SC [10,18]. An alternative interpretation is that critical fluctuations stemming from orbital transition provide the glue of the superconducting pairing [19,20].

*Didier.Jaccard@unige.ch

In this regard, exploration of high-pressure SC in close relatives of $CeCu_2Si_2$ is highly desirable. For such investigation, the isoelectronic and isostructural compound $CeAu_2Si_2$ is an excellent candidate. At ambient pressure, $CeAu_2Si_2$ orders antiferromagnetically below $T_N \approx 10$ K. A previous high-pressure study of a polycrystalline sample, carried out down to 1.2 K, shows that while the magnetic order disappears around 16 GPa, SC does not occur below 19.5 GPa [21].

In this paper, we report on pressure-induced SC in high-quality $CeAu_2Si_2$ single crystals with T_c reaching 2.5 K observed from high-pressure "multiprobe" (transport and calorimetry) measurements up to 27.4 GPa. Unexpectedly, the resulting pressure-temperature phase diagram reveals a highly unusual interplay of superconductivity with magnetism, and differs markedly from that of all known Ce-based pressure-induced superconductors. In particular, for the first time, both superconductivity and magnetism are enhanced with increasing pressure over a broad pressure region. We present a comparison of the unit-cell volume phase diagram of $CeAu_2Si_2$ with that of $CeCu_2Si_2$ and $CeCu_2Ge_2$ and discuss the implication of these results on the pairing mechanism. First-principles calculations show the existence of an intermediate state in the pressure dependence of the Ce-4f orbital occupancy for $CeAu_2Si_2$, which may be a key ingredient for understanding the peculiar behavior in this compound.

II. METHODS

We grow single crystals of $CeAu_2Si_2$ by the "flux" method (see Ref. [22] for guidelines) using Au-Si self-flux and Sn flux. The starting materials are Ce (99.99%) from Ames Lab [23], Au (99.999%), Si (99.9999%), and Sn (99.9999%) from Alfa-Aesar. In the self-flux method, elements with a ratio of $Ce_{0.05}Au_{0.475}Si_{0.475}$ are melted in an alumina crucible inside a sealed evacuated quartz ampoule, held at 1120 °C for 6 h, followed by a slow cooling at 1.2 °C/h down to 850 °C. In the Sn-flux method, which is slightly different from that described in Ref. [24], an ingot of $Ce:Au:Si = 1:20:3$ is presynthesized by arc melting under an argon atmosphere and flipped five times to ensure homogeneity. Big pieces of the crushed ingot are melted with Sn ($CeAu_{20}Si_3:Sn = 1:50$) in an alumina crucible inside a sealed evacuated quartz ampoule, held at 1150 °C for 48 h, followed by a slow cooling at 1 °C/h down to 650 °C. In both cases, crystals, separated from the flux by centrifugation, exhibit well-developed facets and have sizes of up to a few cubic millimeters. Phase impurities are not detected by XRD nor by SEM-EDX measurements. The ambient-pressure measurements show that, within the uncertainty of the geometrical factor, the difference between the Sn-flux and the self-flux samples' resistivity values is almost temperature independent, and their respective residual resistivities are 1.8 and 12.2 $\mu\Omega$ cm.

High-pressure experiments are performed in a Bridgman-type sintered diamond anvil pressure cell using steatite as the pressure-transmitting medium and lead (Pb) as the pressure gauge [25]. A photograph of the actual setup is shown in Fig. S1 of the Supplemental Material [26]. The $CeAu_2Si_2$ sample, arranged in such a way that the c axis is parallel to the compressive force, is connected in series with the Pb for four-probe resistivity measurements. The ac-calorimetry measurements and data analysis are carried out according to the method described in Ref. [27]. The chromel wire, which otherwise serves as one of the voltage leads, is used as the heater and is thermally excited by an ac current of frequency ω while the sample temperature oscillations are detected by measuring the voltage of the Au/AuFe thermocouple V_{ac} at a frequency of 2ω. The data recorded at frequencies above and well below the cutoff frequency correspond, respectively, to a signal dominated by the sample contribution, which can be considered to be inversely proportional to the heat capacity, and to a measure of the mean elevation of the sample temperature over that of the bath. Note that the resistance of the chromel wire is almost pressure independent and more than 2 orders of magnitude larger than that of the sample. Hence, the possibility that the observed anomalies are due to the drastic change in heating power can be ruled out. Throughout the experiments, the pressure gradient estimated from the width of the Pb superconducting transition is $\Delta p \leq 0.3$ GPa. After depressurization, examination of the pressure chamber shows that the distance between the voltage leads has increased by less than 10%. This, together with the geometrical factor uncertainty as well as the change in the sample volume under pressures, sets a 15% error on the absolute resistivity value.

Theoretical calculations are performed based on a combination of electronic structure and dynamical mean-field theory (DMFT) methods, which takes into account both the local atomic physics and correlation effects in the Ce f shell as well as the physical effects of hybridization with conduction electrons [renormalization of crystal-field (CF) levels and Kondo screening] [20]. Our self-consistent (over the charge density) implementation of this method is that of Refs. [28,29] and uses the full-potential linear-augmented plane-wave electronic structure Wien2k [30] code. The DMFT quantum impurity problem is solved with the continuous-time quantum Monte Carlo (CTQMC) method [31] based on the TRIQS library [32] package.

The Wannier orbitals representing Ce-4f states are constructed from the Kohn-Sham states within the energy range from -12.4 to 5.4 eV using the projective approach of Ref. [28]. The local Coulomb interaction between Ce-4f electrons is approximated by a spherically symmetric density-density form parametrized by the Slater parameter $F_0 = U = 6.36$ eV [33] and Hund's rule coupling $J = 0.7$ eV used previously in Ref. [20]. The fully-localized-limit form of the double-counting correction term is employed throughout.

We use the eigenstates $|\Gamma\rangle$ of Ce^{3+}, obtained by diagonalizing the *ab initio* crystal-field and spin-orbit Hamiltonian, as a basis for CTQMC calculations. Rather small off-diagonal elements of the DMFT hybridization function in the $\{\Gamma\}$ basis are neglected. This approximation allows us to treat the full Ce-4f shell and to access low temperatures using the fast "segment picture" algorithm of the CTQMC method [31]. The DMFT quantum impurity problem is solved using up to 4×10^{11} CTQMC moves with a measurement performed after each 200 moves. The calculations are performed for the body-centered tetragonal $ThCr_2Si_2$-type structure at the experimental value of the lattice parameters determined as a function of pressure in Refs. [34–36].

III. RESULTS AND DISCUSSION

A. Experimental results of $CeAu_2Si_2$

The general trend of the electrical resistivity of the investigated $CeAu_2Si_2$ single crystals as a function of pressure (p) and temperature (T) (see Fig. S2 of the Supplemental Material [26]) is typical of Ce-based Kondo lattice systems [9]. However, our samples show a 30 times lower residual resistivity ($\sim$1.8 $\mu\Omega$ cm at $p = 0$) than reported previously [21]. The temperature dependence

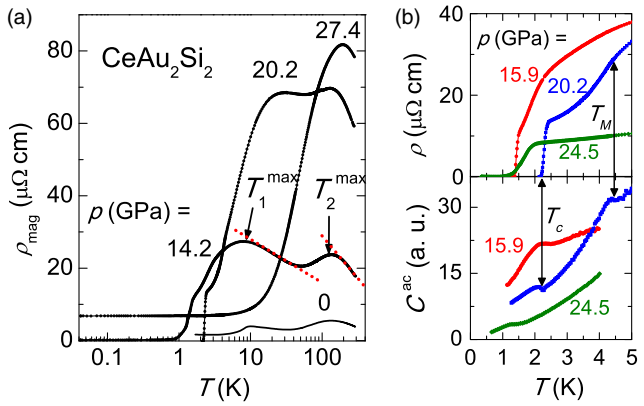

FIG. 1. (a) Logarithmic temperature dependence of the magnetic contribution ρ_{mag} to the in-plane resistivity of $CeAu_2Si_2$ for typical pressures. The two characteristic maxima T_1^{max} and T_2^{max} at 14.2 GPa are marked by the arrows. The dotted red lines are a guide to the eyes, showing the $-\ln T$ dependence of the resistivity. Note that with increasing pressure, T_1^{max} increases drastically while T_2^{max} remains almost constant, and finally the two maxima merge into a single peak. (b) Comparison of the resistivity ρ and heat capacity C^{ac} (in arbitrary unit) for three different pressures at which complete resistive superconducting transitions were observed. A jump in C^{ac} due to SC coincides with the completeness of the resistive transition at 20.2 and 24.5 GPa, but is absent at 15.9 GPa. At 15.9 and 20.2 GPa, the jump in C^{ac} above T_c accompanied by a change in the slope of ρ indicates the magnetic ordering. As an example, two arrows show that at 20.2 GPa the jumps in C^{ac} correspond well to the magnetic transition ($T_M \sim 4.5$ K) and to the completeness of the resistive transition($T_c^{\rho=0} \sim 2.2$ K).

of the magnetic contribution ρ_{mag} to resistivity at representative pressures, shown in Fig. 1(a), is obtained by subtracting the phonon contribution approximated as a pressure-independent term $\rho_{ph} \approx 0.062T$ ($\mu\Omega$ cm) [37] from the raw data. Below room temperature, the ambient-pressure curve already unveils two anomalies of weak magnitude. One can discern a maximum at $\sim$140 K, as well as the onset of a low-temperature anomaly, which is masked by the sharp drop in resistivity ascribed to the magnetic ordering below $T_N \approx 10$ K. At an intermediate pressure of 14.2 GPa, these anomalies have grown markedly and $\rho_{mag}(T)$ exhibits two characteristic maxima at temperatures $T_1^{max} \approx 8$ K and $T_2^{max} \approx 137$ K. Above each of these maxima, $\rho_{mag}(T)$ follows specific $-\ln T$ dependencies, which reflect the incoherent Kondo scattering of the ground state and excited crystal-field levels, respectively [38]. When increasing pressure up to 20.2 GPa, the Kondo scattering keeps increasing. The temperature T_2^{max} remains almost unchanged, while T_1^{max} has by now started its rise. At the highest measured pressure of 27.4 GPa, the two maxima have already merged. The contribution at T_1^{max} dominates in such a way that a single peak is observed at $\sim$200 K. Connected to this behavior, the $-\ln T$ resistivity slope becomes steeper with increasing pressure, which is interpreted as resulting from a dramatic rise in Kondo temperature (T_K) of $2\frac{1}{2}$ orders of magnitude over the investigated pressure range [38].

For the first time, signatures of both superconducting and magnetic transitions are observed in resistivity and heat capacity measurements of $CeAu_2Si_2$, as exemplified in Fig. 1(b) (see also Fig. S3 of the Supplemental Material [26]). It can be seen that at 20.2 GPa, the resistive superconducting transition around 2.2 K coincides with a jump ($\sim$20% of the total signal) in $C^{ac}(T)$, indicating bulk SC. Such an anomaly due to SC is detected at pressures as high as 24.5 GPa. By contrast, at 15.9 GPa, despite the sharp and complete resistive transition, no corresponding anomaly is detected in $C^{ac}(T)$, indicating that SC is likely filamentary or textured [39]. It is worth noting that at 15.9 and 20.2 GPa, the jump in heat capacity together with the downward change of slope in resistivity (distinctively above T_c) are evidence of the persistence of a magnetic ordering, presumably of antiferromagnetic nature. In line with common practice [40], the superconducting and magnetic-ordering temperatures T_c and T_M in $C^{ac}(T)$ are defined by the midpoint of the respective jumps when considering entropy conservation. As an example, the two up-down arrows show that at 20.2 GPa the two midpoints agree well with the completeness of the resistive transition ($T_c^{\rho=0} \sim 2.2$ K) and the onset of downward curvature in the resistivity ($T_M \sim 4.5$ K), respectively.

The pressure dependencies of both T_M and T_c define the phase diagram shown in Fig. 2(a), which reveals several remarkable new features. Even though the magnetism persists up to $\sim$22 GPa, SC is found over the very broad

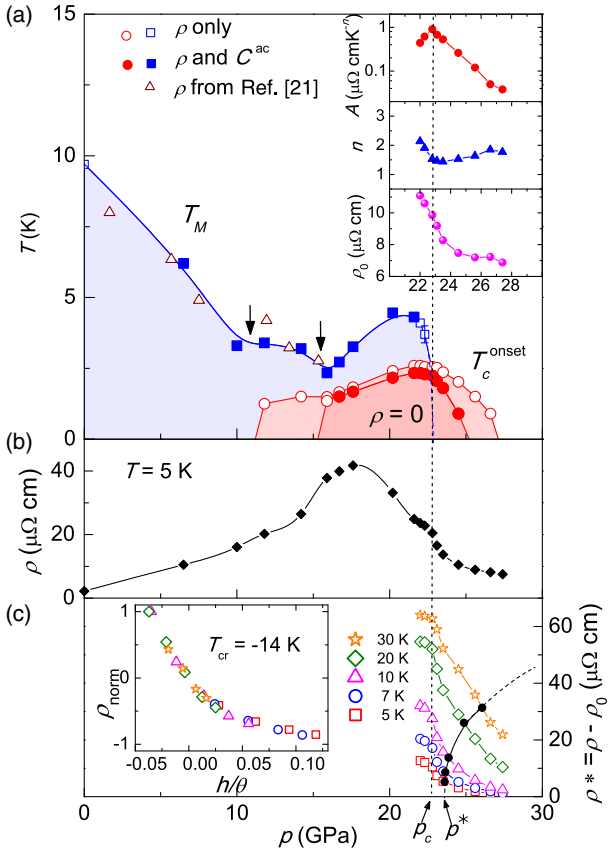

FIG. 2. (a) Experimental p-T phase diagram of $CeAu_2Si_2$. T_c^{onset} and T_M represent the superconducting transition onset and the magnetic ordering temperatures, respectively. The open (closed) symbols denote the data extracted from only the resistivity measurements (from both resistivity and heat capacity measurements). The data from Ref. [21] are also included for comparison, and a good agreement is found. The two arrows mark the anomalies in the $T_M(p)$ curve at ~11 and ~16 GPa, in accordance with the emergence of filamentary and bulk SC. The inset shows the fitting parameters of the power law $\rho(T) = \rho_0 + AT^n$ to the resistivity data above T_c plotted as a function of pressure. The A coefficient reaches a maximum and the temperature exponent n exhibits a minimum at $p_c \approx 22.5$ GPa, where the magnetic order disappears. (b) Plot of ρ versus p at 5 K. The data exhibit one peak at ~17 GPa (onset of bulk SC) and a shoulder at $\sim p_c$. (c) Plot of $\rho^* = \rho - \rho_0$ versus p at selected temperatures up to 30 K. The solid black circles indicate the 50% drop of ρ^* compared to its value at 22.8 GPa for each isotherm. The inset shows the collapse of all normalized data ρ_{norm} when plotted against the generalized distance h/θ from the critical end point located at $p^* \approx 23.6$ GPa and $T_{\text{cr}} = 14$ K (see text for details). The two critical pressures p_c and p^* are indicated by labeled arrows.

pressure range 11.8–26.5 GPa, resulting in a giant overlap of the two phases. At low pressure, T_M first displays a linear-in-T decrease due to the increase of the Kondo coupling, in agreement with previous data [21], but at higher pressures, T_M shows an atypical nonmonotonic dependence, whose anomalies are clearly connected to SC. Indeed, the emergence of filamentary and bulk SC each correspond to a strengthening of magnetism, which manifests itself in the T_M evolution by a flattening and a cusp, respectively. These anomalies may signal the formation of new magnetic phases [41]. In the pressure interval 11.8–15.9 GPa, where T_c onset increases while T_M decreases, SC appears to compete with magnetism as usually observed [6]. However, at higher pressures up to 20.2 GPa, there is a dramatic rise of the T_M from ~2.5 to ~4.5 K. Remarkably, this rise corresponds to a reduction of the heat capacity anomaly. Moreover, in the same pressure range, the bulk T_c also increases strongly (by a similar factor) from ~1.4 to ~2.3 K while the width of the resistive transition remains narrow ($\Delta T_c < 0.3$ K). Consequently, it is unlikely that SC and magnetic order originate from separated phases. Such a simultaneous enhancement of both T_M and T_c over a broad pressure range has never been reported in any other Ce-based pressure-induced superconductors.

With increasing pressure above 21.6 GPa, the signature of magnetic ordering is present only in resistivity, and T_M (see Fig. S4 of the Supplemental Material [26] for its determination) decreases rapidly and drops to zero between 22.3 and 22.8 GPa, indicating a magnetic quantum critical point (QCP) at $p_c = 22.5 \pm 0.3$ GPa. Correspondingly, the fitting of the power law $\rho(T) = \rho_0 + AT^n$ to the resistivity data above T_c, where ρ_0 is the residual resistivity, yields a maximum A coefficient and a minimum exponent ($n \approx 1.5$) at p_c, both of which are standard signatures of a QCP [see Fig. 2(a), inset]. Note that the uncertainty in p_c is comparable to the pressure gradient inside the pressure chamber, and thus, the phase transition could be weakly first order, which raises questions about the quantum nature of p_c. On the other hand, at pressures below 22 GPa, the power-law analysis is not pertinent due to the strong magnetic contribution to the resistivity below T_M. In order to highlight the ground-state excitations independently of magnetic ordering, we plot the isothermal resistivity at 5 K, i.e., just above T_M for $p > 7$ GPa, versus pressure, as shown in Fig. 2(b). Clearly, the resistivity at 5 K shows a broad peak of high magnitude at around 17 GPa, which roughly coincides with the local minimum in T_M and the onset of bulk SC. This observation supports the existence of a putative QCP around the pressure at which the maximum scattering rate occurs. At p_c, only a weak anomaly is seen whose magnitude is smaller than the term $AT^{1.5}$ (with $T = 5$ K), as expected.

Slightly below p_c, T_c reaches a maximum of ~2.5 K, which is among the highest values reported to date for Ce-based HF superconductors. In order to further characterize the superconducting state, we measure the resistive transition at 22.3 GPa under various magnetic fields (B) applied along the crystal's c axis (see Fig. S5 of the Supplemental Material [26]). The results show a very large initial slope of the upper critical field $(dB_{c2}/dT)_{T_c} = -7.1$ T/K, and given that $|dB_{c2}/dT|_{T_c} \propto m^{*2}T_c$ [42], a very large effective mass $m^* \sim 110m_0$ (m_0 is the free-electron mass) is

obtained, confirming heavy-fermion SC. Furthermore, using the extrapolated upper critical field at zero temperature $B_{c2}(0) \sim 9.2$ T, the Ginzburg-Landau (GL) coherence length ξ_{GL} is estimated as $\xi_{GL} = \sqrt{\Phi_0/2\pi B_{c2}(0)} \approx 55$ Å, where Φ_0 is the flux quantum. Preliminary measurements show that $(dB_{c2}/dT)_{T_c}$ scales with T_c.

Just above the pressure p_c, in parallel with the decrease of T_c, the low-temperature isothermal resistivity $\rho^*(p) = \rho(p) - \rho_0(p)$ goes down steeply with increasing pressure, as shown in Fig. 2(c). This behavior is reminiscent of what is found in the vicinity of the second critical point of $CeCu_2Si_2$ around 4.5 GPa, a behavior that is analyzed assuming an underlying critical end point located at (p_{cr}, T_{cr}) in the p-T plane [12]. Following the same data treatment, we define the normalized resistivity $\rho_{norm}(p) = [\rho^*(p) - \rho^*(p_{50\%})]/\rho^*(p_{50\%})$, where for each temperature, $p_{50\%}$ denotes the pressure corresponding to the midpoint of the $\rho^*(p)$ drop compared to its value at 22.8 GPa. As shown in the inset of Fig. 2(b), the ρ_{norm} data below 30 K collapse onto a single curve, when plotted as a function of h/θ, where $h = (p - p_{50\%})/p_{50\%}$ and $\theta = (T - T_{cr})/|T_{cr}|$ with the only free parameter $T_{cr} = -14\,(2)$ K. Such a scaling shows that the resistivity is fully governed by the proximity of a critical end point in a broad region of the p-T plane ($p > p_c$, $T \leq 30$ K). Moreover, the slightly negative T_{cr} value substantiates that $CeAu_2Si_2$ just misses a first-order transition, meaning that only a crossover occurs. By extrapolating the temperature dependence of $p_{50\%}$ to zero temperature, we obtain $p^*(\approx p_{cr}) = 23.6 \pm 0.5$ GPa.

To check the reproducibility of the above results, we perform measurements on $CeAu_2Si_2$ crystals, grown by a self-flux (Au-Si) method (unpublished results). Although the residual resistivity ρ_0 of these crystals is about 5 times higher than that of the present study, the pressures p_c and p^* are found to be almost identical to the aforementioned values, clearly indicating that they are intrinsic and not affected by the sample quality. Around p^*, a scaling of resistivity is also obtained with a slightly more negative T_{cr}. Moreover, we observe a similar resurgence of magnetism for $p > 15$ GPa. However, for the self-flux grown crystals, SC emerges only from 20 GPa and the maximum $T_c \sim 1.1$ K is considerably lower. We attribute this to a strong pair-breaking effect, especially in the magnetic phase, when the electron mean free path $\ell \propto 1/\rho_0$ is short, consistent with observations in $CeCu_2Ge_2$ [9]. This also explains why no SC was detected at all in the previous study, which was performed on polycrystalline samples with an even higher ρ_0 value [21].

B. Comparison with $CeCu_2Si_2$ and $CeCu_2Ge_2$

In order to allow for a straightforward comparison of $CeAu_2Si_2$ and $CeCu_2X_2$ (X = Si or Ge), we convert the pressure into the unit-cell volume (V) of each compound, using high-pressure crystallographic results [34–36] (see the caption of Fig. 3). The three corresponding V-T phase diagrams are shown in Fig. 3. Strikingly, despite the very different properties observed at ambient pressure (notably the ambient pressure volume V_0), there is a broad overlap of the bulk superconducting regions of the three compounds, which confirms that the local environment of the Ce ions plays a key role in the occurrence of SC. In particular, the V dependencies of T_c are nearly identical for $CeCu_2X_2$ and their maximum T_c's occur at the same $V^* \approx 158$ Å^3, far away from the volume at which magnetism disappears in $CeCu_2Ge_2$ and in good agreement with a previous report [43]. This excellent match resembles the one obtained for the magnetic phase diagrams of $CePd_2Si_2$ and $CePd_2Ge_2$, when plotted versus their V [44].

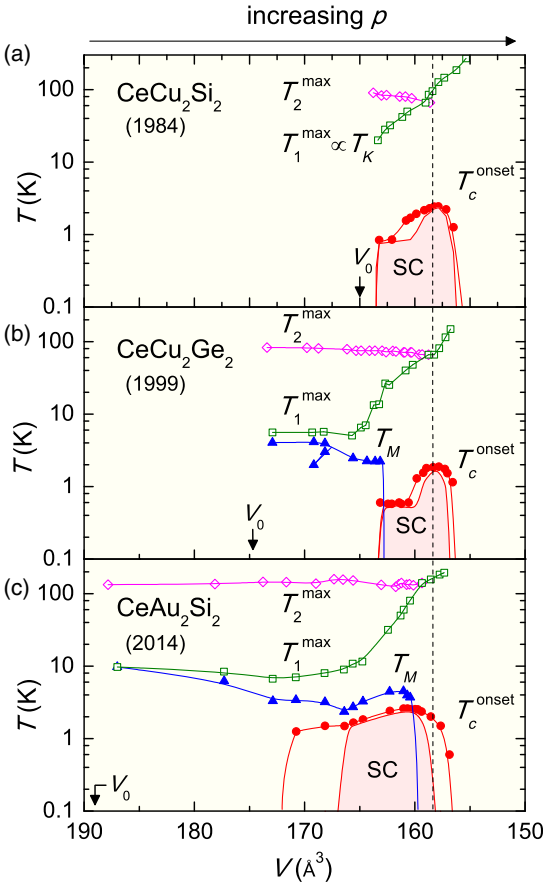

FIG. 3. (a) $CeCu_2Si_2$, (b) $CeCu_2Ge_2$, and (c) $CeAu_2Si_2$. Data for $CeCu_2Ge_2$ and $CeCu_2Si_2$ are taken from Refs. [9,12], respectively. The unit-cell volumes (V_0) at ambient pressure and room temperature for each compound are indicated by the arrows. The small temperature dependence (within 1.2%) of the unit-cell volume has been taken into account as described in note 1 of the Supplemental Material [26], and thus the data for each compound at ambient pressure are actually located at a volume smaller than V_0. Note that for the three compounds the two resistivity maxima merge ($T_1^{max} = T_2^{max}$) and also T_c reaches its maximum near the same volume of 158 Å^3, as indicated by the vertical dashed line. In comparison with $CeCu_2X_2$, in $CeAu_2Si_2$ the SC emerges at a larger V (~171 Å^3), but the magnetic order persists down to a smaller V (~160 Å^3).

For $CeAu_2Si_2$, the maximum T_c is slightly shifted to a larger V. This shift of about 2 Å^3 seems beyond experimental error and might indicate the limit of our comparison in terms of the unit-cell volume. Since we compare isostructural and isoelectronic compounds, the unit-cell volume is certainly a relevant parameter, although it is not ideal. For instance, when pressure reduces the V of $CeAu_2Si_2$ to that of $CeCu_2Si_2$, the Au and Cu atoms may still contribute differently to the crystal-field effect.

The phase diagram of $CeAu_2Si_2$ exhibits two qualitative differences with that of $CeCu_2X_2$. First, SC emerges deep inside the magnetic region. Second, magnetic ordering persists down to a smaller V, and its disappearance coincides with the maximum T_c. This latter characteristic, which is the most common case for Ce-based pressure-induced superconductors, can be taken as strong evidence that SC in $CeAu_2Si_2$ is mediated by critical spin fluctuations [6]. The fact that the onsets of filamentary and bulk SCs correlate with the anomalies in the T_M evolution [see also Fig. 2(a)], hinting at the existence of two putative QCPs, points to a deep link between SC and magnetic instabilities. However, the simultaneous enhancement of both SC and magnetic order in a wide volume (pressure) range, which has never been seen in any other Ce-based pressure-induced superconductors, can hardly be explained by this scenario. Instead, it is plausible that SC and magnetic order are not intrinsically related phenomena, although the possibility that SC develops from the magnetic-ordered state cannot be excluded. This is further corroborated by the comparison of $CeAu_2Si_2$ and $CeCu_2X_2$, made in Fig. 3, which shows that a similar maximum T_c occurs regardless of the presence or the absence of a magnetic QCP. Thus, it appears that another pairing mechanism is involved at least on the low-volume side of the superconducting region.

Another interesting clue pointing in this last direction is found in Fig. 3: for all three compounds, the maximum T_c occurs when the temperatures $T_1^{\max}$ and $T_2^{\max}$ of the resistivity maxima [as defined in Fig. 1(a)] merge, at relatively high temperature ($\sim 40 T_c^{\max}$). Notice that in $CeAu_2Si_2$, $T_1^{\max}$ joins $T_2^{\max}$ at a slightly larger V than that for $CeCu_2X_2$, similar to the small V shift observed for the T_c maximum. Since the three quantities are measured at each pressure run, their correspondence is unaffected by the uncertainty of pressure determination and hence significant. Although the exact relationships are yet to be determined, it is empirically known that the temperatures $T_1^{\max}$ and $T_2^{\max}$ scale approximately with the Kondo temperature (T_K) and CF splitting energy, respectively [45]. In our case, $T_1^{\max}$ gives an indication of T_K only for $V < 165$ Å^3 (i.e., $T_1^{\max} > 10$ K) when the low-temperature resistivity maximum is free from the influence of magnetic ordering. As can be seen in Fig. 3, for $V < 165$ Å^3, $T_1^{\max}$ ($\propto T_K$) shows a nearly exponential increase with decreasing V and appears as the driving parameter of the system, which makes it evolve from long-range magnetic-ordered states, through SC, towards a strongly delocalized paramagnetic f metal at reduced volume. Therefore, we conclude that the superconducting pairing is strongest when Kondo and CF splitting energy scales become comparable. Moreover, $T_1^{\max}$ governs the ground-state excitations reflected by the low-temperature resistivity in the paramagnetic phase. For $CeCu_2X_2$, the relationship $T_1^{\max} \propto 1/\sqrt{A}$ (where A is the Fermi liquid resistivity coefficient) is shown to be fulfilled, except around p^*, where A abruptly drops by 1 order of magnitude [10]. Hence, above p_c, the A values of $CeAu_2Si_2$ [see inset of Fig. 2(a)] are similar to those of $CeCu_2X_2$ taken at the same V. Finally, we note that in comparison with $CeCu_2X_2$, $T_2^{\max}$ of $CeAu_2Si_2$ is almost 2 times higher, and $T_1^{\max}$ shows a slower rise for V just below 165 Å^3, which could account for the persistence of magnetism according to Doniach's simple scheme [46]. In passing, we remark that for $CePd_2Si_2$, SC also occurs when both Kondo resistivity and crystal-field contribution peaks merge [44,47]. It can be conjectured that this feature is a generic property of Ce-based HF superconductors.

In previous publications, the high-pressure superconducting dome of $CeCu_2X_2$ was interpreted within the framework of the critical valence fluctuation theory [10,48,49]. According to this approach, the critical end point of the valence transition line of the Ce ion lies at a pressure p_v and a temperature $T_{\rm cr}$ close to 0 K. This theory provides a consistent interpretation of most of the features observed in the vicinity of p_v, which include, besides SC, a collapse of the resistivity associated with a T-linear regime, an enhanced residual resistivity, and the above-mentioned merging of the two temperatures $T_1^{\max}$ and $T_2^{\max}$ [10,11,49]. However, around p_v, calculations predict a strong decrease of the Ce-4f orbital occupancy with increasing p, while x-ray absorption measurements show a considerably smaller variation (by a factor of 5) [18]. This disagreement and the clue that at the maximum T_c the energy scale of the system is of the order of the CF splitting energy drew us to examine the role played by the orbital states and the associated fluctuations of the Ce-4f electrons in the properties of these materials [19,20].

C. Comparison to dynamical mean-field theory calculations

As a first step to address this issue, we perform calculations based on a combination of electronic structure and DMFT [50] methods, along similar lines as in Ref. [20] for $CeCu_2Si_2$. In a tetragonal crystal field, the $^2F_{5/2}$ ground-state multiplet of the Ce^{3+} ion is split into three doublets: $|0\rangle = a|\pm 5/2\rangle + \sqrt{1-a^2}|\mp 3/2\rangle$, $|1\rangle = |\pm 1/2\rangle$, and $|2\rangle = \sqrt{1-a^2}|\pm 5/2\rangle - a|\mp 3/2\rangle$. A key difference between $CeAu_2Si_2$ and $CeCu_2Ge_2$ is already apparent from our results calculated at ambient pressure and lowest pertinent temperature (7 K). While for both compounds

the ground state is associated with state $|0\rangle$, the first excited state is $|1\rangle$ in $CeAu_2Si_2$ but $|2\rangle$ in $CeCu_2Ge_2$. In order to fully take into account the hybridization and Kondo effects, this splitting can be obtained from the location of the respective Kondo peaks in the orbitally resolved spectral functions. For $CeAu_2Si_2$, we obtain levels $|1\rangle$ and $|2\rangle$ to be, respectively, 9.8 and 24.5 meV above the main Kondo peak associated with state $|0\rangle$, in reasonable agreement with the reported experimental values of 17 and 21 meV [51]. By contrast, for $CeCu_2Ge_2$, we find these splitting to be 34 and 19 meV, respectively. Note that for $CeCu_2Ge_2$, the ambient-pressure ground state has been experimentally ascribed to state $|2\rangle$, although this identification is based on simulations of the temperature dependence of the uniform magnetic susceptibility with the CF levels treated as quasiatomic levels neglecting hybridization and Kondo effects [52].

Correspondingly, another key difference between $CeCu_2Ge_2$ and $CeAu_2Si_2$ is that the occupation of state $|1\rangle$ at ambient pressure is very small for the former while it is sizable for the latter, as displayed on Fig. 4 (upper panels). In this figure, we plot the evolution of the occupancies of each state as a function of pressure for the two compounds. For $CeCu_2Ge_2$, the occupancy of state $|1\rangle$ remains negligible at all pressures, but a transition between a regime dominated by state $|0\rangle$ at low pressure and a regime dominated by state $|2\rangle$ at high pressure takes place, with the occupancy of the two levels crossing each other around 17 GPa. Across the transition region, the f electron weight is transferred from the CF state $|0\rangle$ to the excited level $|2\rangle$, due to the latter's stronger hybridization with itinerant electrons. This "orbital transition" is quite similar to the one recently discussed theoretically [19,20] for $CeCu_2Si_2$, except that it is shifted to higher pressure by about 15 GPa in the Ge-based compound. In contrast, the pressure evolution in the upper panel of Fig. 4 clearly displays *three* distinct regimes: one dominated by state $|0\rangle$ at low pressure (roughly below 10 GPa), one dominated by state $|2\rangle$ at high pressure ($\gtrsim$20 GPa), and an additional intermediate regime (roughly between 10 and 20 GPa) where all three states contribute. We have also followed the evolution of these three regimes as a function of temperature, and the result is visualized in Figs. 4(c) and 4(d) as a color map in the (p, T) plane.

Although our calculations are not performed in the phase with magnetic long-range order, our results do hint at a qualitatively different behavior of the two compounds, as observed experimentally. It is tempting, in particular, to relate the three different regimes found for $CeAu_2Si_2$ to the observed persistence and revival of magnetism in the 15–20 GPa range, and possibly to the existence of several different magnetic phases (as suggested by the kinks and nonmonotonic behavior of the magnetic transition temperature T_M versus pressure). In contrast, in $CeCu_2Ge_2$, one observes a single magnetic phase that collapses at a significantly lower pressure than the maximum of the SC dome. Moreover, the pressure evolution of the Kondo temperature T_K ($\propto T_1^{\max}$) in $CeAu_2Si_2$ (Fig. 3) is different than in $CeCu_2Ge_2$, with an intermediate slower increase in the range 10–16 GPa. Indeed, this is consistent with our calculated evolution of the effective mass, which displays a slow decrease in the intermediate regime, followed by a faster one when state $|2\rangle$ dominates (Fig. S6 of the Supplemental Material [26]).

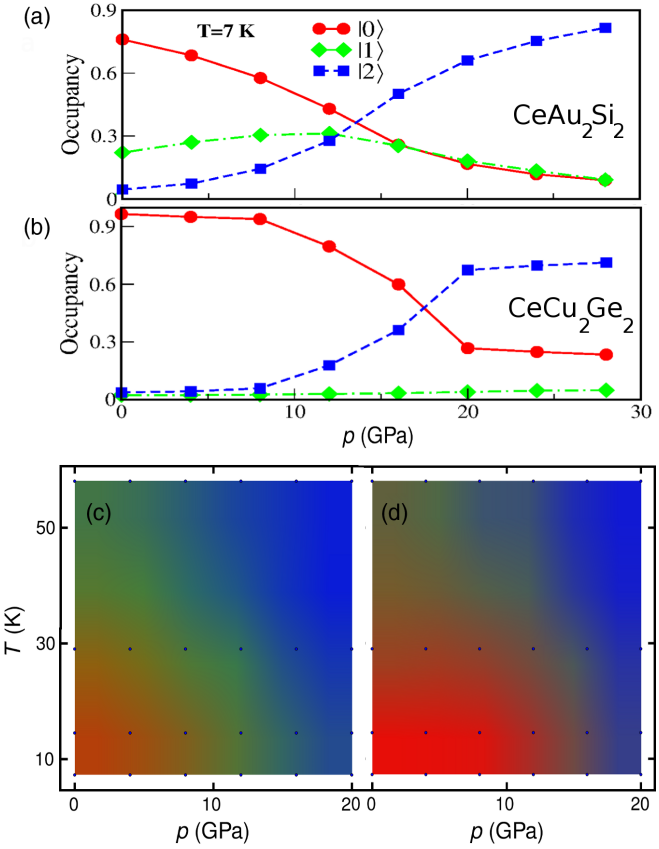

FIG. 4. (a) The calculated occupancy of the CF states $|0\rangle$ (circles), $|1\rangle$ (diamonds), and $|2\rangle$ (squares) as a function of pressure at $T = 7$ K for $CeAu_2Si_2$. The curves are linear interpolations between the corresponding points. (b) The same data for $CeCu_2Ge_2$. (c),(d) The calculated (T, p) maps of the orbital occupancies for $CeAu_2Si_2$ and $CeCu_2Ge_2$, respectively. The color is defined by a RGB code in which the red, blue, and green contributions are proportional to the occupancies n_0, n_2, and the sum of occupancies of two nondominant states, respectively. Hence, the states $|0\rangle$ and $|2\rangle$ clearly dominate in the red and blue areas, respectively, while in the green region, the occupancies of all three states are comparable. The dots indicate the values of T and p for which the LDA + DMFT calculations were performed.

IV. SUMMARY AND CONCLUSION

The above results underline the role of orbital physics in $CeAu_2Si_2$ and $CeCu_2X_2$. The critical end point, identified at (p_{cr}, T_{cr}) through the scaling of the resistivity around p^* in $CeAu_2Si_2$, as well as previously in $CeCu_2Si_2$ [12], can be

that of an orbital transition line, first described by Hattori [19] and in agreement with our calculations (see also Ref. [20]). In these systems, only a crossover regime is realized because the temperature T_{cr} is slightly negative. However, T_{cr} is small enough that the charge or orbital fluctuations associated with the orbital crossover are sufficiently developed to mediate both the non-Fermi liquid properties of the normal phase and the superconducting pairing. In $CeAu_2Si_2$, magnetism and superconductivity may originate from the occupancy of different CF levels in the intermediate-pressure region according to our calculations. The increase of Kondo scale induced by the orbital transition may drive the collapse of magnetism, explaining its sudden disappearance and hence the proximity of the pressures p_c and p^*, as opposed to the case of $CeCu_2X_2$ for which these two pressures are well separated. As discussed in Sec. III B, it appears that spin fluctuations are not the driving force for superconductivity in $CeAu_2Si_2$. Still, it remains challenging to understand the giant overlap of SC and magnetism and, in particular, the striking relationship $T_c \propto T_M$ observed in a broad pressure range, which definitely require further studies.

In conclusion, $CeAu_2Si_2$ is discovered to be a new HF superconductor under a very broad pressure interval from 11.8 to 26.6 GPa. Within approximately two-thirds of this interval, SC appears below the magnetic phase transition. Intriguingly, when increasing pressure from 16.7 to 20.2 GPa, both bulk T_c and T_M are strongly enhanced, and almost proportional. T_c reaches its maximum value of $\sim$2.5 K slightly below the pressure $p_c \approx 22.5$ GPa, where magnetic order disappears. The scaling behavior of resistivity indicates a continuous delocalization of Ce-4f electrons associated with a critical end point lying just above p_c. The T_c maximum occurs when the Kondo and CF energies are similar and at almost the same unit-cell volume as for $CeCu_2Si_2$ and $CeCu_2Ge_2$, providing a clue to the pairing mechanism. First-principles calculations indicate the existence of an intermediate state in the Ce-4f orbital occupancy in $CeAu_2Si_2$, which might be related to its peculiar behavior in comparison with its close relatives $CeCu_2X_2$. Nevertheless, we emphasize that the understanding of the newly observed behavior in $CeAu_2Si_2$ remains largely open [53]. Future experimental investigations of the isoelectronic compounds $CeAg_2Si_2$, or even $CeAu_2Ge_2$ and $CeAg_2Ge_2$, will likely enrich the debate. On the theoretical side, calculations of various Ce-based systems are highly desirable in order to extend comparisons with the already rich experimental results. For example, an interesting issue is the very weak pressure response of the intermediate valence compound $CePd_3$ [54].

ACKNOWLEDGMENTS

We acknowledge discussions with M. Ferrero, P. Hansmann, and J.-P. Rueff, technical assistance from M. Lopes, and financial support from the Swiss National Science Foundation through Grant No. 200020-137519 and the European Research Council under Grant No. ERC-319286 QMAC. Computing resources were provided by the Swedish National Infrastructure for Computing (SNIC) at the National Supercomputer Centre (NSC) and PDC Center for High Performance Computing and by the Swiss Center for Scientific Computing.

[1] D. Jaccard, K. Behnia, and J. Sierro, *Pressure Induced Heavy Fermion Superconductivity in* $CeCu_2Ge_2$, Phys. Lett. A **163**, 475 (1992).

[2] F. M. Grosche, S. R. Julian, N. D. Mathur, and G. G. Lonzarich, *Magnetic and Superconducting Phases of* $CePd_2Si_2$, Physica (Amsterdam) **223–224B**, 50 (1996).

[3] N. D. Mathur, F. M. Grosche, S. R. Julian, I. R. Walker, D. M. Freye, R. K. W. Haselwimmer, and G. G. Lonzarich, *Magnetically Mediated Superconductivity in Heavy Fermion Compounds*, Nature (London) **394**, 39 (1998).

[4] H. Hegger, C. Petrovic, E. G. Moshopoulou, M. F. Hundley, J. L. Sarrao, Z. Fisk, and J. D. Thompson, *Pressure-Induced Superconductivity in Quasi-2D* $CeRhIn_5$, Phys. Rev. Lett. **84**, 4986 (2000).

[5] E. D. Bauer, H. O. Lee, V. A. Sidorov, N. Kurita, K. Gofryk, J.-X. Zhu, F. Ronning, R. Movshovich, J. D. Thompson, and T. Park, *Pressure-Induced Superconducting State and Effective Mass Enhancement near the Antiferromagnetic Quantum Critical Point of* $CePt_2In_7$, Phys. Rev. B **81**, 180507(R) (2010).

[6] G. Knebel, D. Aoki, and J. Flouquet, *Antiferromagnetism and Superconductivity in Cerium Based Heavy-Fermion Compounds*, C.R. Phys. **12**, 542 (2011).

[7] F. Steglich, J. Aarts, C. D. Bredl, W. Lieke, D. Meschede, W. Franz, and H. Schafer, *Superconductivity in the Presence of Strong Pauli Paramagnetism:* $CeCu_2Si_2$, Phys. Rev. Lett. **43**, 1892 (1979).

[8] B. Bellarbi, A. Benoit, D. Jaccard, J. M. Mignot, and H. F. Braun, *High-Pressure Valence Instability and* T_c *Maxium in Superconducting* $CeCu_2Si_2$, Phys. Rev. B **30**, 1182 (1984).

[9] D. Jaccard, H. Wilhelm, K. Alami-Yadri, and E. Vargoz, *Magnetism and Superconductivity in Heavy Fermion Compounds at High Pressure*, Physica (Amsterdam) **259–261B**, 1 (1999).

[10] A. T. Holmes, D. Jaccard, and K. Miyake, *Signatures of Valence Fluctuations in* $CeCu_2Si_2$ *under High Pressure*, Phys. Rev. B **69**, 024508 (2004).

[11] D. Jaccard and A. T. Holmes, *Spin and Valence-Fluctuation Mediated Superconductivity in Pressurized Fe and* $CeCu_2(Si/Ge)_2$, Physica (Amsterdam) **359–361B**, 333 (2005).

[12] G. Seyfarth, A.-S. Ruetschi, K. Sengupta, A. Georges, D. Jaccard, S. Watanabe, and K. Miyake, *Heavy Fermion Superconductor* $CeCu_2Si_2$ *under High Pressure: Multi-probing the Valence Crossover*, Phys. Rev. B **85**, 205105 (2012).

[13] E. Vargoz and D. Jaccard, *Superconducting and Normal Properties of* $CeCu_2Ge_2$ *at High Pressure*, J. Magn. Magn. Mater. **177–181**, 294 (1998).

[14] H. Q. Yuan, F. M. Grosche, M. Deppe, C. Geibel, G. Sparn, and F. Steglich, *Observation of Two Distinct Superconducting Phases in* $CeCu_2Si_2$, Science **302**, 2104 (2003).

[15] O. Stockert, J. Arndt, E. Faulhaber, C. Geibel, H. S. Jeevan, S. Kirchner, M. Loewenhaupt, K. Schmalzl, W. Schmidt, Q. Si, and F. Steglich, *Magnetically Driven Superconductivity in* $CeCu_2Si_2$, Nat. Phys. **7**, 119 (2011).

[16] P. Monthoux, D. Pines, and G. G. Lonzarich, *Superconductivity without Phonons*, Nature (London) **450**, 1177 (2007).

[17] S. Kittaka, Y. Aoki, Y. Shimura, T. Sakakibara, S. Seiro, C. Geibel, F. Steglich, H. Ikeda, and K. Machida, *Multiband Superconductivity with Unexpected Deficiency of Nodal Quasiparticles in* $CeCu_2Si_2$, Phys. Rev. Lett. **112**, 067002 (2014).

[18] J.-P. Rueff, S. Raymond, M. Taguchi, M. Sikora, J.-P. Itie, F. Baudelet, D. Braithwaite, G. Knebel, and D. Jaccard, *Pressure-Induced Valence Crossover in Superconducting* $CeCu_2Si_2$, Phys. Rev. Lett. **106**, 186405 (2011).

[19] K. Hattori, *Meta-Orbital Transition in Heavy-Fermion Systems: Analysis by Dynamical Mean Field Theory and Self-Consistent Renormalization Theory of Orbital Fluctuations*, J. Phys. Soc. Jpn. **79**, 114717 (2010).

[20] L. V. Pourovskii, P. Hansmann, M. Ferrero, and A. Georges, *Theoretical Prediction and Spectroscopic Fingerprints of an Orbital Transition in* $CeCu_2Si_2$, Phys. Rev. Lett. **112**, 106407 (2014).

[21] P. Link and D. Jaccard, *Pressure Induced Heavy-Fermion Behavior of* $CeAu_2Si_2$ *near 17 GPa*, Physica (Amsterdam) **230–232B**, 31 (1997).

[22] P. C. Canfield and Z. Fisk, *Growth of Single Crystals from Metallic Fluxes*, Philos. Mag. B **65**, 1117 (1992).

[23] Materials Preparation Center, Ames Laboratory, U. S. DOE Basic Energy Sciences, http://www.mpc.ameslab.gov.

[24] Y. Ota, K. Sugiyama, Y. Miyauchi, Y. Takeda, Y. Nakano, Y. Doi, K. Katayama, N. D. Dung, T. D. Matsuda, Y. Haga, K. Kindo, T. Takeuchi, M. Hagiwara, R. Settai, and Y. Onuki, *Electrical and Magnetic Properties of* $CeAu_2Si_2$, J. Phys. Soc. Jpn. **78**, 034714 (2009).

[25] A. T. Holmes, D. Jaccard, G. Behr, Y. Inada, and Y. Onuki, *Unconventional Superconductivity and Non-Fermi Liquid Behavior of ϵ-Iron at High Pressure*, J. Phys. Condens. Matter **16**, S1121 (2004).

[26] See Supplemental Material at http://link.aps.org/supplemental/10.1103/PhysRevX.4.031055 for more data and analysis.

[27] A. T. Holmes, Ph. D. thesis, Université de Genève, 2004 [http://archive-ouverte.unige.ch/unige:284].

[28] M. Aichhorn, L. Pourovskii, V. Vildosola, M. Ferrero, O. Parcollet, T. Miyake, A. Geroges, and S. Biermann, *Dynamical Mean-Field Theory within an Augmented Plane-Wave Framework: Assessing Electronic Correlations in the Iron Pnictide LaFeAsO*, Phys. Rev. B **80**, 085101 (2009).

[29] M. Aichhorn, L. Pourovskii, and A. Georges, *Importance of Electronic Correlations for Structural and Magnetic Properties of the Iron Pnictide Superconductor LaFeAsO*, Phys. Rev. B **84**, 054529 (2011).

[30] P. Blaha, K. Schwarz, G. Madsen, D. Kvasnicka, and J. Luitz, *WIEN2k, An Augmented Plane Wave+Local Orbitals Program for Calculating Crystal Properties* (Technische Universität Wien, Austria, 2001).

[31] E. Gull, A. J. Millis, A. I. Lichtenstein, A. N. Rubtsov, M. Troyer, and P. Werner, *Continuous-Time Monte Carlo Methods for Quantum Impurity Models*, Rev. Mod. Phys. **83**, 349 (2011).

[32] M. Ferrero and O. Parcollet, *TRIQS: A Toolbox for Research on Interacting Quantum Systems*, http://ipht.cea.fr/triqs.

[33] Our estimates within the constrained LDA method for $CeCu_2Si_2$, $CeCu_2Ge_2$, and $CeAu_2Si_2$ give values of F_0 differing by less than 0.2 eV. Hence, the value previously used for $CeCu_2Si_2$ has been adopted for the two other compounds.

[34] A. Onodera, S. Tsuduki, Y. Ohishi, T. Watanuki, K. Ishida, Y. Kitaoka, and Y. Onuki, *Equation of State of* $CeCu_2Ge_2$ *at Cryogenic Temperature*, Solid State Commun. **123**, 113 (2002).

[35] S. Tsuduki, A. Onodera, K. Ishida, Y. Kitaoka, A. Onuki, N. Ishimatsu, and O. Shimomura, *Synchrotron X-Ray Diffraction and Absorption Studies of* CeM_2X_2 *(M = Cu, Ni and X = Si, Ge) at High Pressure*, Solid State Commun. **134**, 747 (2005).

[36] M. Ohmura, K. Sakai, T. Nakano, H. Miyagawa, G. Oomi, I. Sato, T. Komatsubara, H. Aoki, Y. Matsumoto, and Y. Uwatoko, *Anisotropic Lattice Compression and Possible Valence Change in Kondo Compound* $CeAu_2Si_2$, J. Magn. Soc. Jpn. **33**, 31 (2009).

[37] The phonon contribution ρ_{ph} is well approximated by a linear-in-T term above $\Theta_D/10$, where Θ_D is the Debye temperature. From specific heat data of Ref. [24], $\Theta_D \approx 270$ K is obtained. Below $\Theta_D/10 \approx 27$ K, the linear term overestimates ρ_{ph}. However, the low-T resistivity is dominated by the magnetic contribution even at low pressure, and thus the subtraction of a small linear term has weak effect on our data analysis. Under pressure, ρ_{ph} is expected to decrease slightly, but in comparison to the strong increase of the magnetic resistivity, it can be taken as pressure independent.

[38] B. Cornut and B. Coqblin, *Influence of the Crystalline Field on the Kondo Effect of Alloys and Compounds with Cerium Impurities*, Phys. Rev. B **5**, 4541 (1972).

[39] T. Park, H. Lee, I. Martin, X. Lu, V. A. Sidorov, K. Gofryk, F. Ronning, E. D. Bauer, and J. D. Thompson, *Textured Superconducting Phase in the Heavy Fermion* $CeRhIn_5$, Phys. Rev. Lett. **108**, 077003 (2012).

[40] N. Tateiwa, Y. Haga, T. D. Matsuda, S. Ikeda, T. Yasuda, T. Takeuchi, R. Settai, and Y. Onuki, *Novel Pressure Phase Diagram of Heavy Fermion Superconductor* $CePt_3Si$ *Investigated by ac Calorimetry*, J. Phys. Soc. Jpn. **74**, 1903 (2005).

[41] S. Seo, V. A. Sidorov, H. Lee, D. Jang, Z. Fisk, J. D. Thompson, and T. Park, *Pressure Effects on the Heavy-Fermion Antiferromagnet* $CeAuSb_2$, Phys. Rev. B **85**, 205145 (2012).

[42] T. P. Orlando, E. J. McNiff, Jr., S. Foner, and M. R. Beasley, *Critical Fields, Pauli Paramagnetic Limiting, and Material Parameters of* Nb_3Sn *and* V_3Si, Phys. Rev. B **19**, 4545 (1979).

[43] T. C. Kobayashi, K. Fujiwara, K. Takeda, H. Harima, Y. Ikeda, T. Adachi, Y. Ohishi, C. Geibel, and F. Steglich, *Valence Crossover of Ce Ions in* $CeCu_2Si_2$ *under High Pressure—Pressure Dependence of the Unit Cell Volume and the NQR Frequency*, J. Phys. Soc. Jpn. **82**, 114701 (2013).

[44] H. Wilhelm and D. Jaccard, *Calorimetric and Transport Investigations of* $CePd_{2+x}Ge_{2-x}$ *($x = 0$ and 0.02) up to 22 GPa*, Phys. Rev. B **66**, 064428 (2002).

[45] Y. Nishida, A. Tsuruta, and K. Miyake, *Crystalline-Electric-Field Effect on the Resistivity of Ce-Based Heavy Fermion Systems*, J. Phys. Soc. Jpn. **75**, 064706 (2006).

[46] S. Doniach, *The Kondo Lattice and Weak Antiferromagnetism*, Physica (Amsterdam) **91B+C**, 231 (1977).

[47] A. Demuer, A. T. Holmes, and D. Jaccard, *Strain Enhancement of Superconductivity in* $CePd_2Si_2$ *under Pressure*, J. Phys. Condens. Matter **14**, L529 (2002).

[48] K. Miyake, *New Trend of Superconductivity in Strongly Correlated Electron Systems*, J. Phys. Condens. Matter **19**, 125201 (2007).

[49] A. T. Holmes, D. Jaccard, and K. Miyake, *Valence Instability and Superconductivity in Heavy Fermion Systems*, J. Phys. Soc. Jpn. **76**, 051002 (2007).

[50] A. Georges, G. Kotliar, W. Krauth, and M. J. Rozenberg, *Dynamical Mean-Field Theory of Strongly Correlated Fermion Systems and the Limit of Infinite Dimensions*, Rev. Mod. Phys. **68**, 13 (1996).

[51] T. Willers, Ph. D. thesis, Universität zu Köln, 2011.

[52] G. Knopp, A. Loidl, K. Knorr, L. Pawlak, M. Duczmal, R. Caspary, U. Gottwick, H. Spille, F. Steglich, and A. P. Murani, *Magnetic Order in a Kondo Lattice: A Neutron Scattering Study of* $CeCu_2Ge_2$, Z. Phys. B **77**, 95 (1989).

[53] R. Flint, A. H. Nevidomskyy, and P. Coleman, *Composite Pairing in a Mixed-Valent Two-Channel Anderson Model*, Phys. Rev. B **84**, 064514 (2011).

[54] P. Pedrazzini, D. Jaccard, M. Deppe, C. Geibel, and J. G. Sereni, *Multiprobe High-Pressure Experiments in* $CePd_{0.6}Rh_{0.4}$ *and* $CePd_3$, Physica (Amsterdam) **404B**, 2898 (2009).